33RD CONGRESS
OF THE INTERNATIONAL COUNCIL
OF THE AERONAUTICAL SCIENCES
STOCKHOLM, SWEDEN, 4-9 SEPTEMBER, 2022

ICAS 2022 SWEDEN

# VOLUMETRIC VELOCITY MEASUREMENTS OF A HELICAL VORTEX PAIR

Dominic Schröder[1], Thomas Leweke[2], Ralf Hörnschemeyer[1] & Eike Stumpf[1]

[1]Institute of Aerospace Systems, RWTH Aachen University, 52062 Aachen, Germany
[2]CNRS, Aix-Marseille Université, Centrale Marseille, 13384 Marseille, France

## Abstract

This paper presents the results of an experimental study fn a helical vortex pair which is influenced by centrifugal instability. Volumetric velocity measurements using particle tracking methods are performed in a water channel for a one-bladed rotor in hovering conditions. The vortex pair is generated by a specific tip design which provokes the single tip vortex to split up into two separate vortices. The objective of this modification is to alter the characteristic vortex parameters by means of mutual interactions to minimise the negative effects associated with blade-vortex interactions. Previous studies showed that for selected vortex systems an immediate rapid core growth for both vortices is detected. The reason for this conduct was found in the occurence of centrifugal instabilities affecting both vortices. These instabilities cause a rapid disturbance of the vortex pair resulting in the observed significant core growth. To reveal the three-dimensional characteristics of the instability, volumetric measurements are performed. The results are compared to stereo particle image velocimetry data for validation purposes. Due to the unsteady behaviour, instantaneous snapshots are investigated to detect the secondary vortices caused by the instability. A statistical evaluation shows that the presence of those structures is pronounced in the early wake age, corresponding to the strongest impact of the instability.

**Keywords:** vortex flow, vortex instability, volumetric velocimetry, helical vortex system, rotor wake

## 1 Introduction

The flows encountered in applications involving rotating blades such as e.g. helicopters or wind turbines are characterised by unsteady and three-dimensional flow phenomena. The superposition of concentrated tip vortices, the shear layers shed from the trailing edges of the rotor blades and the influence of the external flow create a highly complex flow field, which strongly affects the rotor aerodynamics. In contrast to the straight vortices emerging behind a plane, the superposition of rotational motion and the freestream velocity causes the tip vortices in the rotor wake to form a helical geometry while being convected downstream. Additional to their decreasing effect on the rotor performance due to the induced drag, these vortices can lead to detrimental fluid-structure interactions. With regard to helicopters, blade-vortex interactions (BVI) causing unwanted vibrations and an impulsive acoustic noise emission pose a limit to the flight envelope of the helicopter [1, 2]. The vehemence of the interactions is mostly affected by the strength of the involved vortex, quantified by the vorticity gradients (concentrated vortices with small core radii posses high gradients in the core regions) and the bound circulation [3, 4]. In wind farms, the concentrated vortices resulting from the turbine upstream have a severe impact on the fatigue characteristics and the general performance [5, 6]. Destabilising the wake would provide a possibility to reduce the aforementioned negative aspects for a variety of applications. Consequently, methods to influence the relevant tip vortex quantities and wake stability characteristics have been the topic of several studies over the past years, e.g. [7, 8,

9]. Active systems involve higher harmonic blade control mechanisms, active trailing edge flaps and active twist mechanisms [10]. Passive systems mainly consist of blade tip geometry modifications to affect the initial vortex system emerging from the trailing edge by splitting up the single concentrated tip vortex into separated vortices. In viscous flow, a vortex pair of two like-signed vortices eventually merge into one single vortex. The outcome yields a significant change of the characteristic parameters comparing the initial two vortices and the final merged vortex. The general vortex structure is spread out, resulting in an increased core radius and a decreased peak vorticity in the vortex centre [11]. A detailed description of the two-dimensional merging procedure is given in [12, 13]. The presence of mutual instability phenenomena, which affect the vortex pair, accelerates the onset of a merging process and further enhances the beneficial effects, such as the widening of the vortex core [14, 11]. Several of the proposed tip designs aim at the generation of more than one vortex and take advantage of their mutual interactions to provoke instability and merging phenomena in the rotor wake, see e.g. [15] for a review of helicopter blade tip shapes. For wind turbines, different blade tip and winglet designs with similar techniques to modify the vortex system are part of current research, an example is given in the study of Ostovan et al. [16]. The results show great potential for both applications, however, many aspects of the underlying physical mechanims are not fully understood yet. New insights in the flow phenomena and the mutual interactions involved in such closely spaced helical vortex systems are the objectives of the French-German research project TWIN-HELIX, which combines theoretical and experimental methods. Comprehensive experimental studies using planar and volumetric velocimetry measurements are carried out to investigate the interaction of two helical vortices. A specific tip design involving a parametric fin mounted on the pressure side is used to split up the single concentrated tip vortex into a vortex pair.

The presented work is the extension of previous experimental studies including stereoscopic particle image velocimetry (SPIV) and dye visualisations, which revealed that an unexpected rapid core growth of both vortices occurs for certain fin configurations which ultimately results into a merged vortex with strongly widened core. [17, 18]. The occurence of those rapid groth rates prior to the onset of merging gave a hint to the presence of instability phenomena in the vortex system. Observations within the conducted visualisations revealed strongly disturbed vortex cores immediately behind the trailing edges confirming the aforementioned statement. Similar to straight vortex pairs (see [19]), the instability mechanisms occurring in helical vortex pairs are divided into two groups, depending on the perturbation wavelength compared to the vortex core diameter. Possible candidates for the investigated vortex systems are the general long-wave instability [20, 21, 7] and the short-wave elliptic and curvature instability [22, 23, 24, 25]. However, the time scales of the observed phenomena causing the rapid core growth were incompatible with the expected long- and short-wave instability mechanisms [25]. An explanation of the behaviour was found in the initial velocity profiles, which showed that both vortices were unstable with respect to centrifugal instability [26, 27]. This instability mechanism arises in vortices when the absolute value of the circulation declines with growing distance from the vortex center, i. e. caused by an accumulation of opposite-signed vorticity surrounding the vortex core [28]. Following the method proposed by Bayly [26], the viscous growth rate of the perturbations and the corresponding most amplified wavelength were obtained, which agreed well with the calculated core growth rates and the observed perturbation scales in the visualisations. The presence of the centrifugal instability showed great potential with respect to the desired effect of the modification, therefore its origin and development requires further investigations. The previous experimental studies contained only planar velocimetry measurements, unable to reveal the three-dimensional character of the perturbations resulting from the instability effects.
Within this contribution, results from volumetric velocity measurements in the rotor wake using particle tracking methods are presented. The initial interaction process and development of the vortex pair influenced by the instability is investigated. To validate the volumetric data, a comparison to previous SPIV measurement campaigns is performed. The instability effect is observed in the formation of secondary structures between the vortices, affecting both vortex cores. Due to their unsteady behaviour, these structures are merely spotted in selected volumetric snapshots, which required the evaluation of all instantaneaous recordings. A qualitative analysis of the secondary vortices is given,

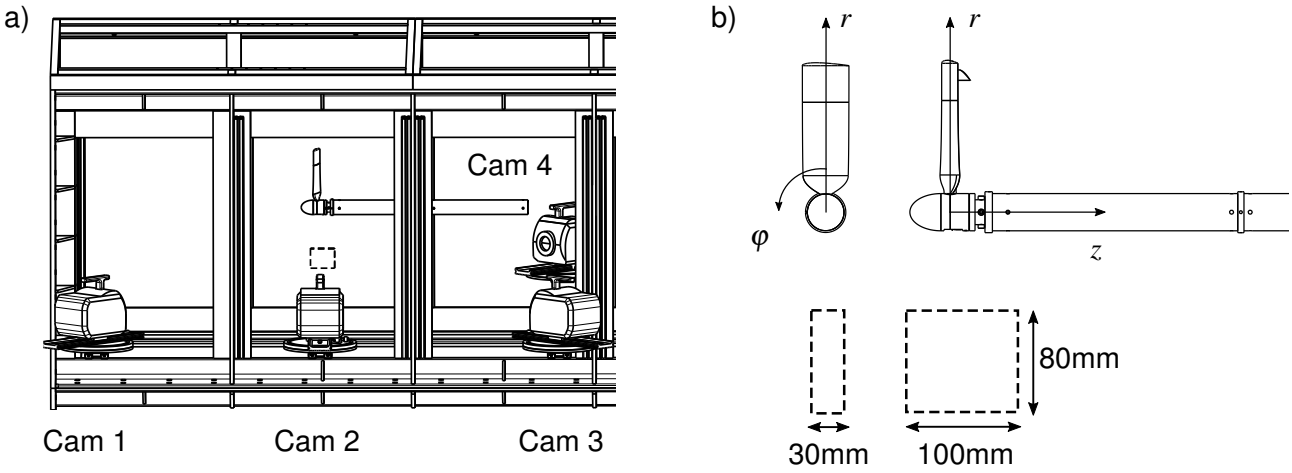


Figure 1 – (a) Schematic of the experimental setup for the particle tracking velocimetry measurements. (b) Global coordinate system for the rotor geometry (free stream is in z-direction) and measurement volume dimensions.

revealing that their presence is pronounced in early wake age. Within this rotor phase interval, a significant increase of both primary vortex core radii is found. These initial effects contribute to a subsequent accelarated growth prior to the onset of the vortex merging.

## 2 Experimental Methods

Experiments were carried out in the large recirculating water channel of the Institute of Aerospace Systems. Its test section has dimensions of 1.5 m (width) $\times$ 1 m (height) $\times$ 6.5 m (length) and glass walls suitable for optical measurement techniques. Due to the reduced tangential velocities in the core regions for equal Reynolds numbers, the quantative analysis of vortical flows in water provides obvious advantages in comparison to air. Since the balance between centrifugal and pressure forces on seeding particles in the vortex cores is much easier to obtain, the recorded particle images are less effected by the well-known seeding void in the vortex core regions, ensuring a valid determination of the vortex core parameters.

A one-bladed rotor of constant chord length (NACA 0012 profile, radius $R = 240\,\mathrm{mm}$, chord $c = 80\,\mathrm{mm}$) equipped with a modified tip geometry was analysed in hover conditions. The blade is slightly twisted and has a rectangular planform. The simple rectangular blade geometry was chosen to focus on the basic mechanisms of generating two tip vortices, a detailed describtion of the design proces is found in [29]. A perpendicular fin mounted on the pressure side in the vicinity of the tip generates the second vortex. The fin has an untwisted NACA 0012 cross section and its geometry is defined by the radial position $d$, height $h$, chord $c_f$ and angle of attack $a_f$. The rotor rotates at a constant rotation rate of $1\,\mathrm{Hz}$, resulting in a Reynolds number on the blade tip of $\mathrm{Re} = c(2\pi f)/\nu = 120000$. To prevent the flow from recirculating around the rotor disc, a small free-stream velocity in the water channel is required to ensure stationary flow conditions. Volumetric particle tracking measurements (PTV) using the "Shake-The-Box" (STB) technology introduced by Schanz et al. [30] were carried out to acquire volumetric flow fields in the rotor wake. Figure 1(a) shows a schematic of the experimental set-up, a system consisting of four cameras (Imager sCMOS, $2048 \times 2048\,\mathrm{px}$ resolution) was used to record the particle images, synchronized triggering is ensured by an optical encoder connected to the rotor shaft. Cubic polyamide particles of mean diameter $50\,\mu\mathrm{m}$ and density $1.016\,\mathrm{g/cm^3}$ were used to seed the flow. To prevent aberrations due to the change of fluids in the optical path, water-filled prisms were used as suggested by Prasad & Jensen [31]. Adapters fulfilling the Scheimpflug criterion were mounted in front of the cameras to ensure a uniformly focussed image. The measurement volume was illuminated by a double-pulsed laser (Quantel Twins Ultra) providing a pulse energy of $120\,\mathrm{mJ}$ at an effective wavelength of $532\,\mathrm{nm}$. The dimensions of the measurement volume and the coordinate system used for the subsequent evaluation are displayed in Fig. 1(b), the center of the measurement volume was positioned directly below the axis of the rotor shaft. In order to track the evolution of the vortices despite the limited dimensions of the measurement region, linear axes are installed to alter

the rotor position in relation to the fixed measurement volume. The previous SPIV studies revealed that the instabilities and the resulting rapid core growth rates occur primarily at early wake ages (rotor angles $\varphi = 10° - 180°$), therefore it was decided to apply the volumetric analysis within this phase interval. Each measurement volume has a thickness $t$ = 30 mm, which covers approximately a rotor phase of $\varphi_{\mathrm{vol}} = 7°$. In total, 26 measurement volumes (300 frames per volume) up to a rotor phase $\varphi_{\mathrm{max}} = 185°$ were recorded in the double-frame/single-pulse acquisition mode. A small overlap of the volumes was established to prevent data loss due to noisy data at the volume edges. The volumes contained $3 \times 10^4 \pm 20\%$ valid particles. Due to the small free-stream velocity in the water channel, a constant seeding density was difficult to sustain for all volumes which explains the deviations in the particle number. A two-sided two-level target was used to calibrate the camera system. The results were refined by the volume self-calibration introduced by Wieneke [32] and a calibration of the optical tranfer function established by Schanz et al. [33]. The commercial PIV/PTV software DaVis 10.0.5 was used for image acquisition, calibration process and subsequent processing of the particle images.

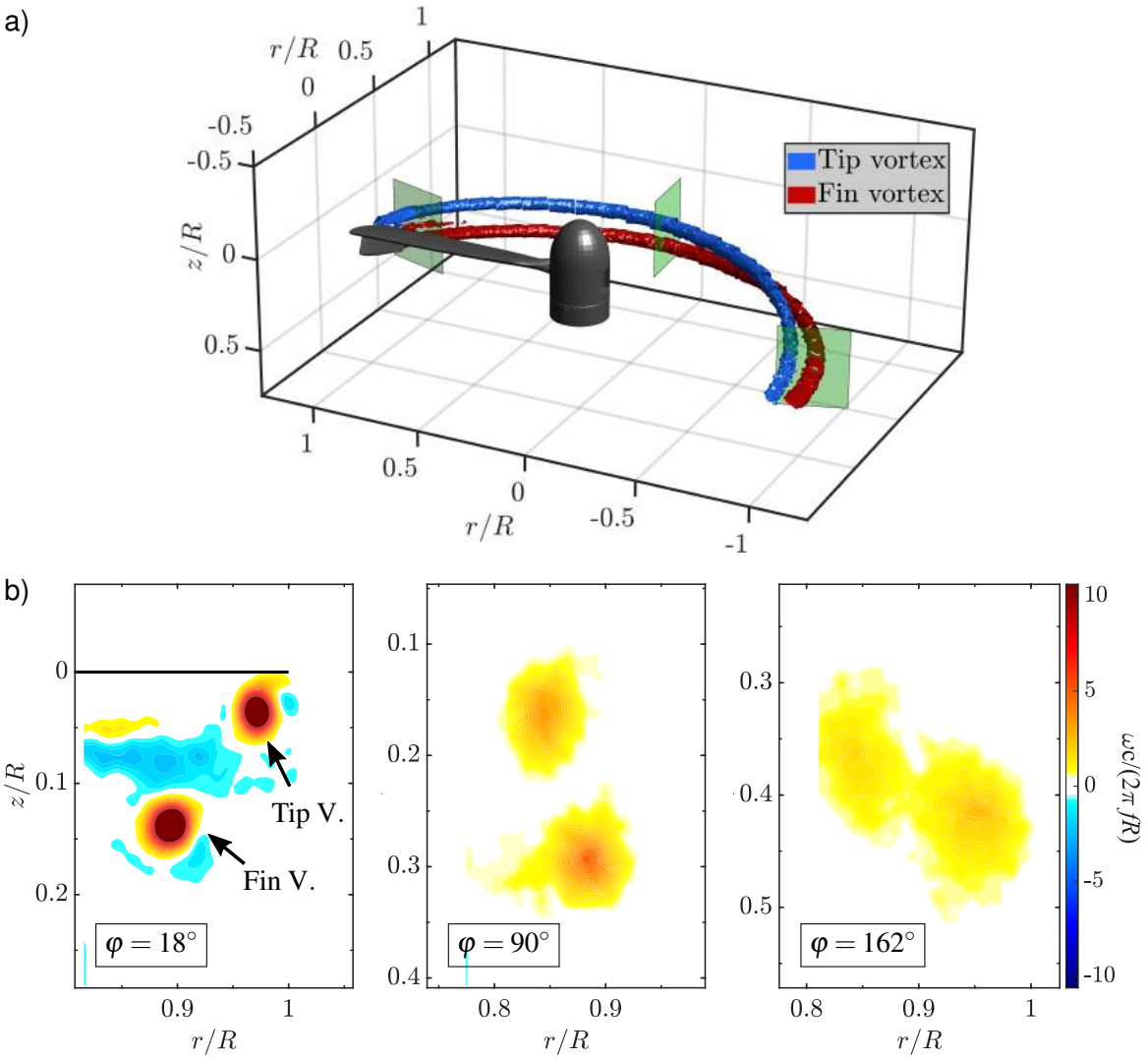


Figure 2 – (a) Volumetric isosurfaces of the normalised azimuthal vorticity component up to a rotor phase of $\varphi = 185°$ for the modified blade (green slices indicate the position of the fieldcuts shown in (b)). (b) Phase-averaged vorticity contours at $\varphi = 18°$, $\varphi = 90°$ and $\varphi = 162°$, black line represents the trailing edge of the blade.

## 3 Results and Discussion

The previous measurement campaigns included a parameter study to detect fin configurations, which create suitable vortex systems for the desired mutual interaction process in the wake, see [17]. Based on the previous results, the configuration which showed the most significant growth rates for both distinct vortices prior to the subsequent vortex merging was identified and chosen for the volumetric analysis. The geometric specifications defining the fin geometry are: $d/c = 0.2$, height $h/c = 0.3$, chord $c_f/c = 0.8$. This configuration produced a vortex system with a slighty stronger fin vortex $(\Gamma_f/\Gamma_t \approx 1.15)$, which ultimately merged into a single vortex with a core growth up to a factor 5 after one rotor revolution in comparison to an unmodified blade. For all recorded volumes, the freestream velocity was set to $u_\infty = 11.4$ cm/s, resulting in a tip speed ratio $\lambda = (2\pi f R)/u_\infty = 13$. Figure 2(a) shows a qualitative impression of the wake generated by the modified blade. To create this representation, the location of each measurement volume in relation to the blade was tracked during the recordings, giving the oppurtunity to align them with respect to the vortex axis detected in the previous volumes. Two distinct vortices emerging from the blade are clearly visible, illustrated by the isosurfaces of the normalised azimuthal vorticity component. The tip vortex is coloured in blue, the fin vortex in red. Phase-averaged data is used to create the isosurfaces displayed in Fig. 2(a). No evident three-dimensional disturbances surrounding the vortices or any wavy perturbations of the cores are visible. These findings confirm the expected unsteady behaviour of the instability, indicating that the evaluation of instantaneous snapshots is required to discover the related effects. The general impact of the instability presence on the wake evolution is exposed by the fieldcuts given in Fig. 2(b), their position in relation to the blade is marked by the green slices in Fig. 2(a). The cuts show contours of the phase-averaged azimuthal vorticity component, demonstrating the development of the vortex system. The roll-up process for both vortices is completed at early wake stages, at a rotor phase of $\varphi = 18°$ two concentrated co-rotating vortices have formed. While moving downstream, the vortices start to rotate around each other, combined with a decrease of core separation and a slight deformation of the vortex structure. Looking at the fields at $\varphi = 90°$ and $\varphi = 162°$, it is evident, that both the core radiii of both vortices are strongly widened and the peak vorticities in the centers significantly decreased, a consequence of the instability and the ongoing merging process.

### 3.1 Comparison between SPIV and Shake-The-Box data

For validation purposes, the obtained volumetric STB results are compared to the data of a previous SPIV campaign. The equipment, rotor model and the flow conditions were identical for both measurements. The SPIV data was recorded up to a rotor phase of $\varphi_{\mathrm{max,SPIV}} = 540°$ in steps of $\Delta\varphi_{\mathrm{SPIV}} = 18°$. Data processing was performed with a final correlation window size of $48 \times 48$ px, with a 75 % overlap. This spatial resolution provided a sufficient amount of 8-10 vectors within the radii of the smallest vortex cores measured in these experiments. In comparison, the particle fields and corresponding Langrangian particle tracks calculated from the STB data allowed a reconstruction to a regular Cartesian grid with a voxel size of $96 \times 96 \times 96$ px with a 75 % overlap, yielding a coarser resolution in comparison. The time-varying seeding density and the low free-stream velocity prevented a finer spatial resolution. With regard to the rotor phase discretization, the STB volumes covered a rotor phase of $\varphi_{\mathrm{vol}} = 7°$, which yields a total of 38 Cartesian field cuts, resulting in a much finer angular resolution of $\Delta\varphi_{\mathrm{STB}} \approx 0.19°$. The following comparison of the calculated vortex data is based on the phase-averaged velocity fields/volumes. A conditional averaging procedure to minimize the effec of vortex wandering on the vortex core profiles (swirl velocities, radius), compare [34, 35], was neglected in the present analysis since it is expected, that the influence of the secondary vortex is dominant in comparison to the impact of vortex wandering.

To extract the relevant parameters characterising the tip vortices, the measured veloctity fields for both measurements have been analysed with the same routines. The vortex centers have been detected utilising the $\lambda_2$-criterion introduced by Jeong&Hussain [36]. Due to the sufficient seeding density within the core regions, no further filtering techniques as e.g. convolution filters [35] were needed for the centre identification. A projection of the velocities on a local polar grid $(\rho, \xi)$ and subsequent averaging the azimuthal component $u_\xi$ for each radius $\rho$ is used to obtain the swirl velocity

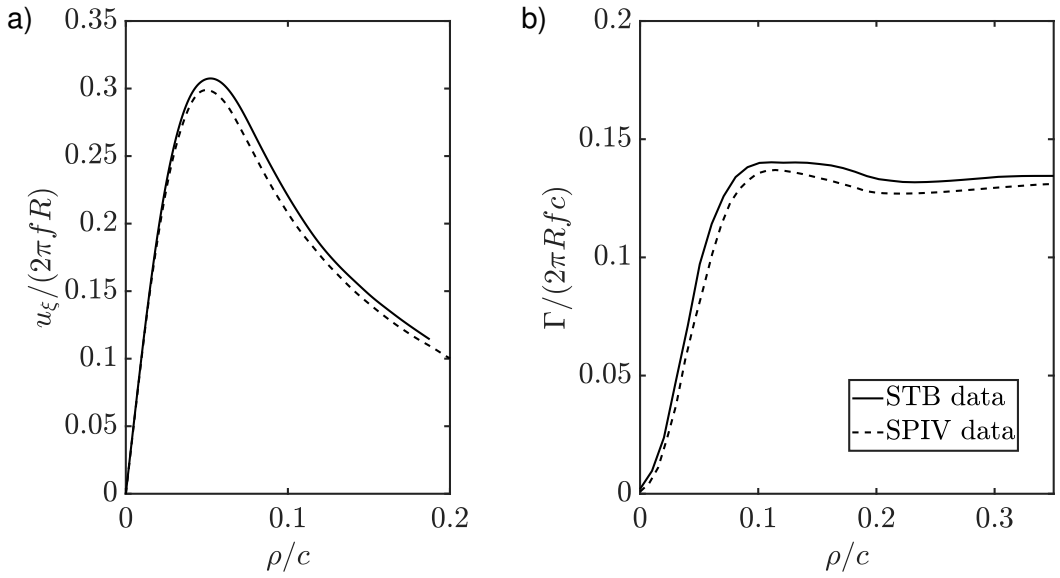


Figure 3 – (a) Radial swirl velocity and (b) radial circulation profiles for the tip vortex at a rotor phase of $\varphi = 18^\circ$. Profiles extracted from both STB and SPIV data.

profiles of a detected vortex. Figure 3(a) shows an example of the deduced swirl profiles for both data sets, the shown profile is extracted from the tip vortex at a rotor phase of $\varphi = 18^\circ$ (compare the vorticity contours in Fig.2(b). Despite the coarser resolution of the STB data, both profiles are in good agreement with each other. The core radii $a_{\max}$, defined as the distance from the vortex centre to the point of maximum swirl velocity, are almost identical. It was expected, that the peak velocities calculated from the STB measurements would yield a reduced value due to the smearing effect of the coarser resolution, which would result in greater differences of the extracted core radii. The second quantity describing the vortices is the circulation and the correspponding ratio within the vortex pair. To determine the value for each vortex, the vorticity field is separated into two distinct polygons, based on the previously detected vortex centers (a detailed description of the procedure is given in [29]). For both regions, the edges of the polygon define the border of the line integral to determine the circulation. An example of a radial circulation profile for SPIV and STB data is presented in Fig. 3(b). It is again extracted from the tip vortex at a rotor phase of $\varphi = 18^\circ$. Similar to the radial swirl profile, the STB data matches the SPIV results quite well. Both profiles show a slight decrease from the maximum value at $\rho/c \approx 0.1$, indicating the presence of counter-rotating vorticity regions in the vicinity of the vortex core, which is the criterion for centrifugal instability. Taking a look at the corresponding contour in Fig.2(b), it is indeed visible, that both vortices are sourrounded by vorticity patches of opposite sign. The effect of the instability on the growth rates of the vortex core radii is clearly visible in the evolution of the core radii, presented in Fig. 4(a). In this diagramm, the equivalent Gaussian core radii $a = a_{\max}/1.12$ is used to allow comparability with theoretical analysis, see [17] for more details. Both fin and tip vortex cores grow significantly before the merging process begins. The SPIV measurements showed that the excessive growth rates for both vortices occur immediately after emerging from the trailing edge, up to vortex ages of $\varphi \approx 160 - 180^\circ$, compare the highlighted region in the smaller diagramm. During the period $\varphi \approx 180 - 270^\circ$, the ongoing merging process hinders a valid extraction of the core radii until the final vortex is formed. It was therefore decided to perform the volumetric measurements within half a rotor revolution to cover the growth phase, which is mainly affected by the instability. Again, both measurements are in good agreement, the data of the STB measurements is extracted for each fieldcut of the volumes, providing a much finer angular resolution of the core growth. In Fig. 4(b), the circulation development during the early wake stage is displayed. As expected, the circulation for both vortices remain nearly constant during the growth phase. The slight decrease at phases $\varphi \approx 120 - 150^\circ$ for the tip vortex (blue) and the corresponding total value (black) in the system is related to a slightly inaccurate position of the rotor in relation to the measurement plane/volume, which caused a partly cut-off tip vortex and consequently

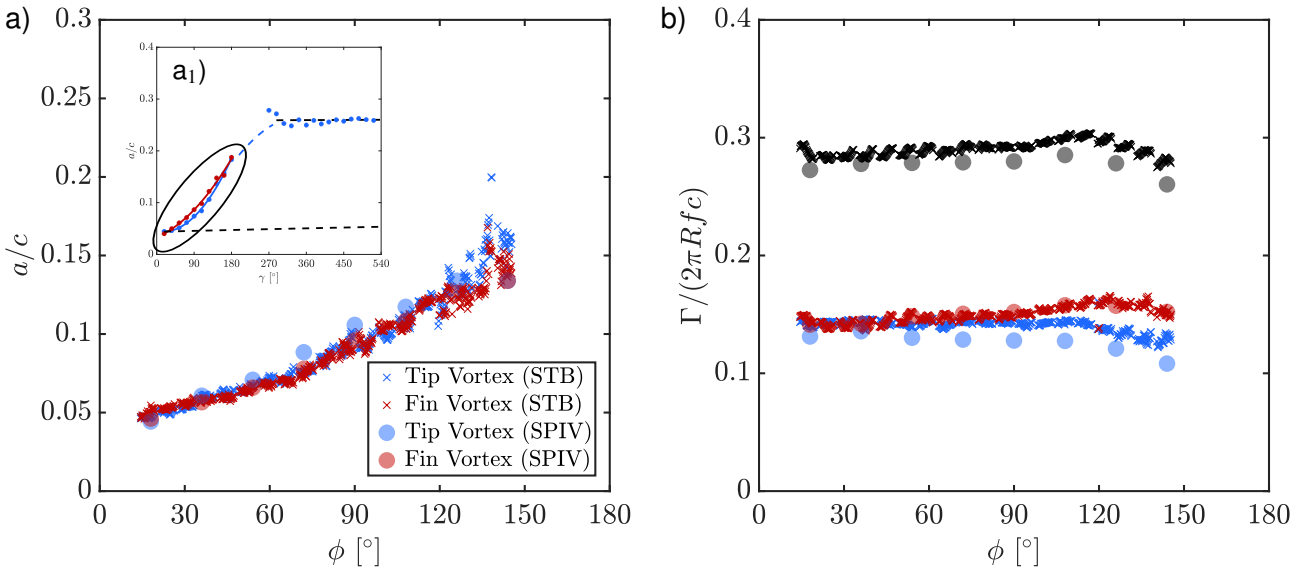


Figure 4 – (a) Gaussian core radii evolution of both vortices in the region of rapid growth (marked with the black elipse within the full SPIV diagram ($a_1$)) for STB and corresponding SPIV data. (b) Circulation values obtained for the distinct vortices and the total field (black).

smaller calculated circulations.

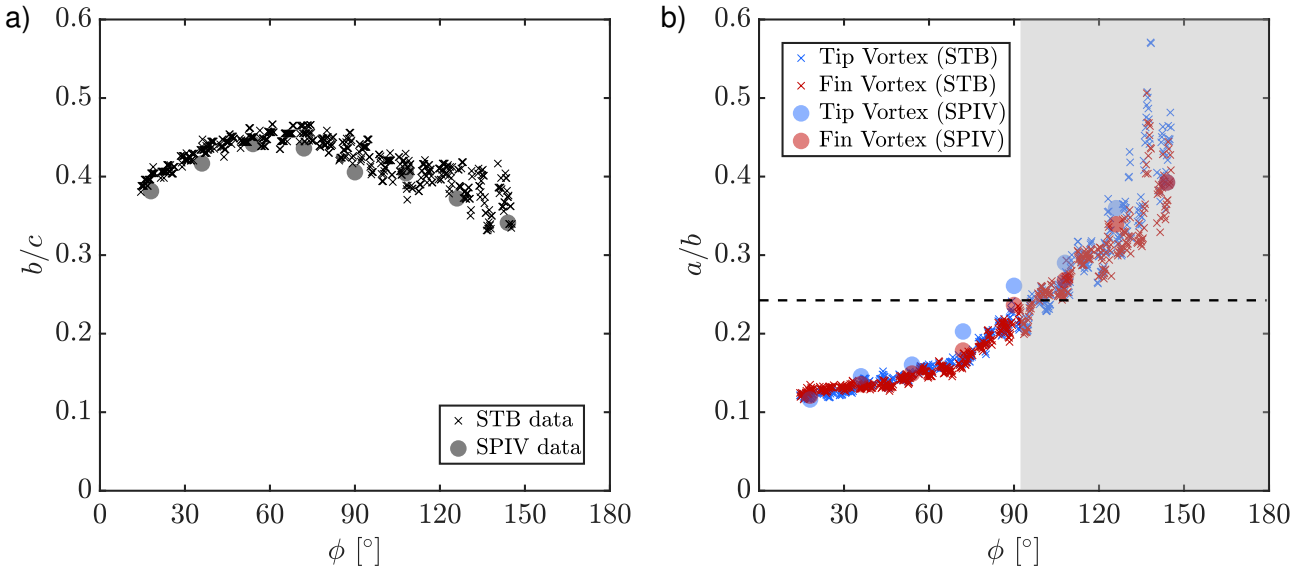


Figure 5 – (a) Development of the vortex core distances for STB and SPIV data. (b) Evolution of the relation between Gaussian core radii and vortex distance $a/b$ for different rotor phases (dashed black line marks the critical ratio of $a/b = 0.24$ determining the onset of vortex merging).

It should be mentioned that the presence of the fin increases the averaged total circulation in comparison to an unmodified blade (not shown here), indicating that the general circulation generated by the blade is enhanced as well [29]. The averaged values for the STB measurements are modestly higher than the corresponding SPIV results. With regard to the merging procedure, the distance between both vortices is of interest, since the relation between the Gaussian core radii $a$ and the vortex distance $b$ is an indicator for the onset of merging [11]. Figure 5(a) displays the development of the distance based on the determined center positions. Up to a rotor phase of $\varphi = 60°$, the separation increases, afterwards both vortices move towards each other. The critical ratio characterising the onset

of merging is given by $a/b = 0.24$ [11]. Figure 5(b) reveals, that this ratio is exceeded at $\varphi = 90°$. For subsequent wake stages, the core growth is expected to be driven by a combination of instability and merging effects. Prior to the beginning of merging, the centrifugal instability is considered as the main contributor. With regard to the evolution of $a/b$, it is evident, that the core growth rates compensate for the expanding vortex distance, yielding a continous increase.
Despite the lower spatial resolution, it can be stated that the STB data is in surprisingly good agreement with the SPIV data, providing an accurate determination of the relevant vortex parameters for this study. The notably increased angular resolution allowed a much finer observation of the parameter evolution in comparison to previous studies. Still, higher seeding densities and consequently more determined particle tracks should be achieved for future measurement campaigns.

## 3.2 Analysis of secondary vortex structures

To get a better understanding of the phenomena caused by the instability, the volumetric data in the early wake stages is investigated in detail. In Fig. 6(a), the position of the measurement volume in relation to the rotor and the local coordinate system used for the following volume analysis is shown. Due to the small coverage of $\varphi_{\mathrm{vol}} = 7°$ and the negligible curvature of the vortices within the volume, no transformation into the rotor hub cylinder coordinates is performed. The results presented in 3.1 were determined using phase-averaged data. However, it is expected, that any occuring unsteady effects related to the instability are smoothed out due to the averaging process, which leaves the phase-averaged volumes unsuitable to detect any secondary structures. The confirmation of this assumption is given in Fig. 6(b), which displays the vortical structure within the phase-averaged volume at a rotor phase $\varphi = 24°$, the isosurfaces represent a positive threshold of the Q-criterion [37]. The tip and fin vortices are clearly visible, their core structure appears relatively undisturbed and no secondary structures are detected in their vicinity. With regard to the immidiate core growth and the appearance of counter-rotating vorticity close to both vortices, compare Fig. 8(b), the influence of the instability should already be present at this wake age. Due to the lack of time-resolved data, single snapshots are used for further examination. The theoretical analysis yields, that the instability causes a wavy perturbation of the vortex cores, the most amplified wavelength can be determined from the velocity fields with the methods described in [26]. This deformation of the internal core structure causes the generation of secondary structures near the vortex cores. It should be stated, that the centrifugal instability is no mutual instability phenomenon. Nevertheless, in the presented case, both vortices fulfill the criterion of a decrease within the radial circulation profile with increasing distance from the vortex center. Consequently, the instability should affect both vortices.

Figure 7(a) shows an instantaneous snapshot of the same measurement volume shown in Figure 6(b), the isosurfaces correspond to the equal threshold of the Q-criterion. In contrast to the

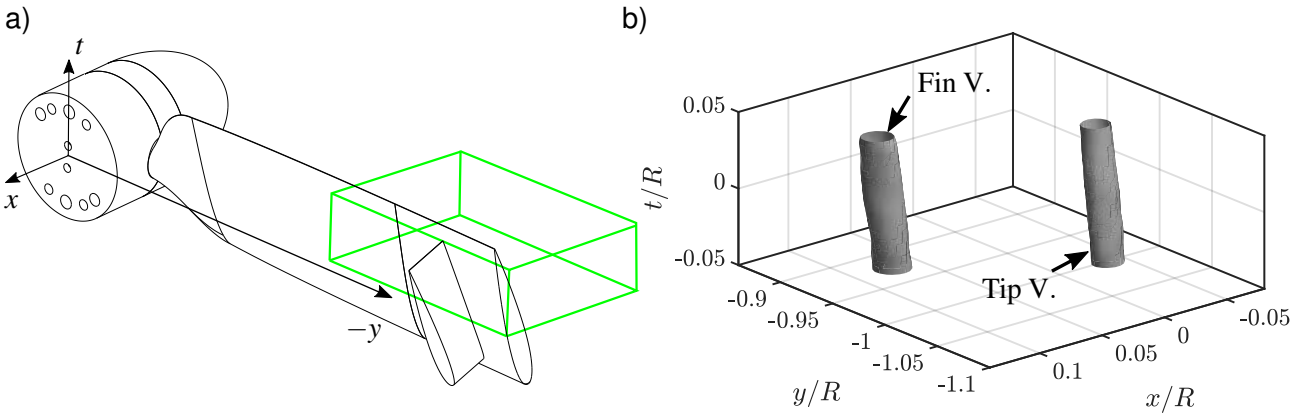


Figure 6 – (a) Sketch of the STB measurement volume in relation to the rotor blade and local coordinate system used for subsequent analysis. (b) Isosurface of the Q-criterion at a rotor phase $\varphi = 24°$ for phase-averaged data.

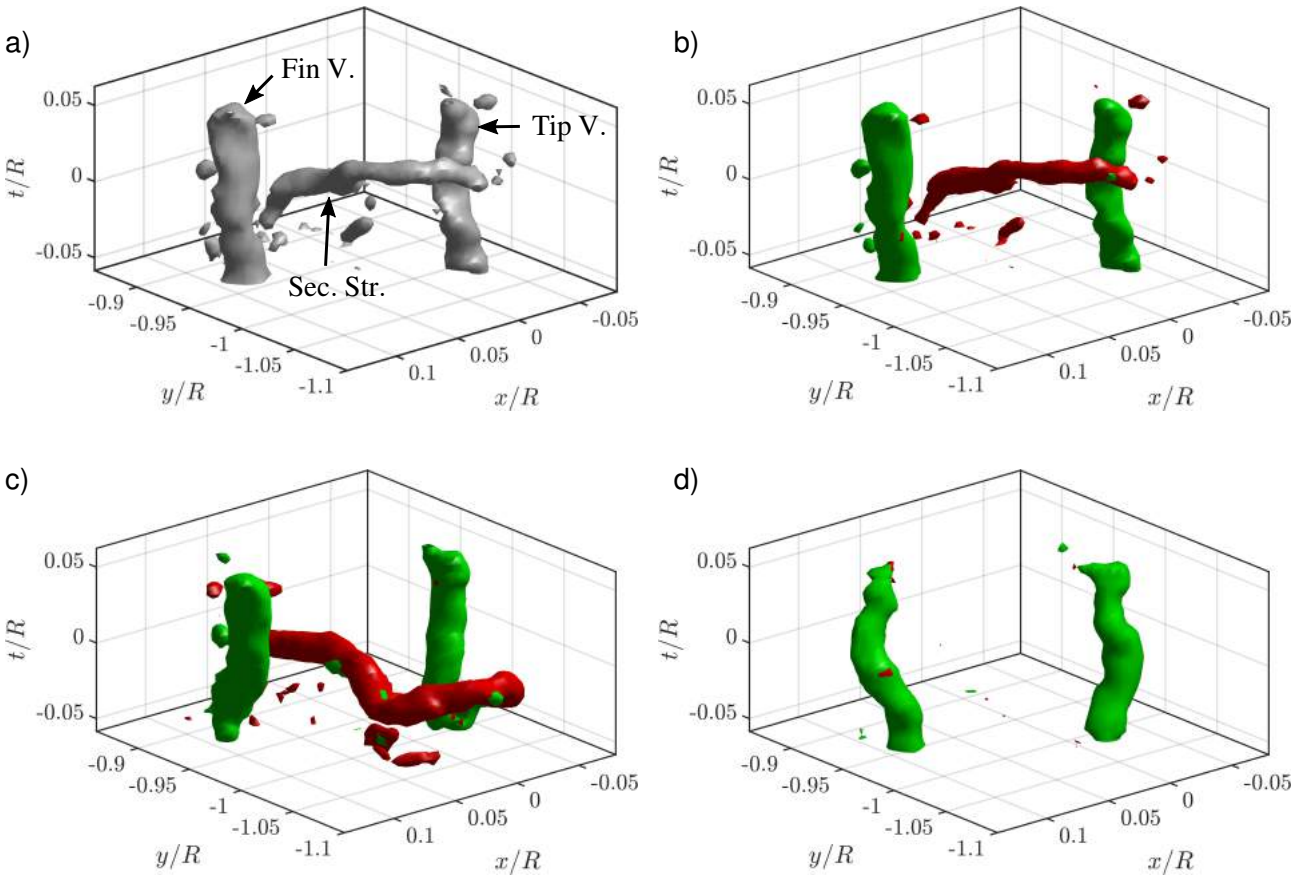


Figure 7 – (a) Instantaneous isosurfaces of the Q-criterion at a rotor phase $\varphi = 24°$. (b) Decomposition of the instantaneous Q-criterion into $Q_{\text{tip}}$ (green) and $Q_{\text{sec}}$ (red). (c-d) Additional examples for instantaneous isosurfaces using the decomposed criteria.

phase-averaged data, a secondary vortex between both primary vortices is indeed detected. Both vortex cores appear disturbed, but the identification of a dominant perturbation wavelength is unfeasible. Unfortunately, it is not possible to track the further evolution of the secondary structure due to its unsteady behaviour. To differentiate between primary vortices and secondary structures, a method introduced by Wolf et al. [38] is used for further evaluation. In their study, they gave the experimental proove for the existence of similar secondary structures entangling the primary tip vortices in a hovering rotor wake, which were previously regarded as a numerical phenomenon. Wolf et al. showed that the generation of those structures has a physical background and is not purely associated to numerical issues. The following methodology is based on their work. The vorticity unit vector is used to decompose the scalar Q-criterion into a Cartesian framework [39]. Within the local coordinate system introduced in Fig. 6(a), it is given by:

$$\omega_n = \begin{pmatrix} \omega_{n,x} \\ \omega_{n,y} \\ \omega_{n,t} \end{pmatrix} = \frac{\nabla \times \vec{v}}{|\nabla \times \vec{v}|} \,. \tag{1}$$

The primary vortices are mainly rotating around the $t$-axis, so the corresponding part of the normalised vorticity vector is used to identify tip and fin vortices with the following criterion:

$$Q_{\text{tip}} = \begin{cases} -\omega_{n,t} \cdot Q; & \omega_{n,t} < 0 \\ 0; & \omega_{n,t} \geq 0 \end{cases} \,. \tag{2}$$

To account for the negative rotational sense of the primary vortices, the negative sign is inserted. The secondary structures are identified using the $y$-component of the normalised vorticity vector, since it is expected, that they mainly form in $y$-direction. The Q-values are multiplied with the projection of $\omega_n$

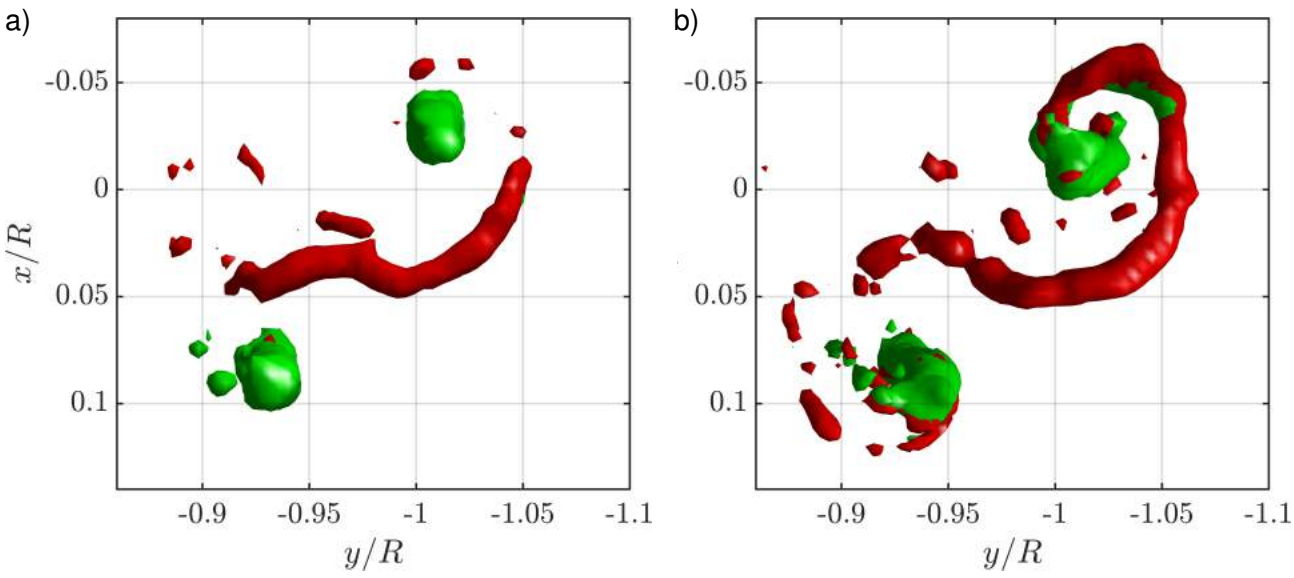


Figure 8 – (a-b) Top view of the decomposed criteria shown in Fig. 7(b-c).

on the xy-plane, which is given by:

$$\omega_{n,xy} = \sqrt{\omega_{n,x}^2 + \omega_{n,y}^2}\,. \tag{3}$$

The criterion to discover the secondary structures yields:

$$Q_{\mathrm{sec}} = \begin{cases} \omega_{n,xy} \cdot Q; & \omega_{n,y} \neq 0 \\ 0; & \omega_{n,y} = 0 \end{cases}\,. \tag{4}$$

A differentiation between the rotational direction of the secondary structures, as done in [38] is neglected in this analysis. It should be stated that only positive tresholds for the Q-values are considered, since only the rotational parts of the flow are of interest here. Due to the sufficient seeding density within the vortex cores, no further filtering procedure is needed. Applying the decomposition to the snapshot displayed in Fig. 7(a) yields the result presented in Fig. 7(b). The primary vortices (coloured in green) are clearly distinguished from the secondary structure (red). Both isosurfaces are created with the equal threshold for $Q_{\mathrm{tip}}$ and $Q_{\mathrm{sec}}$, respectively. The decomposition is applied to all snapshots, which were recorded for the different rotor phases, further examples for $\varphi = 24°$ are given in Fig. 7(c-d). As expected, the manifestation of the secondary structures and their position along the primary vortices' axes is an unsteady phenomenon. Consequently, they are not detected in every snapshot, compare Fig. 7(d), despite a visible deformation of the vortex cores. Determining the characteristic parameters of the secondary structures is impeded by the limited spatial resolution and the influence of the adjacent primary vortices. However, the qualitative impressions given in Fig. 7 suggest that strength and core size of the secondary vortices is similar to the primary ones. A direct comparison to the results from Wolf et. al [38] is problematic considering the completely different blade geometries and flow conditions, still it appears, that the presence of the centrifugal instability and the enhanced perturbations of the vortex cores provoke the generation of more pronounced secondary vortices. A topview of the decomposed isosurfaces, given in Fig. 8, accentuates the geometry of the secondary vortices. It is characterised by an S-shaped layout, entangling both primary vortices. The observed shape is similar to the structures detected between two tip vortices in the experiments conducted by Wolf et al. [38]. Previously conducted visualizations, see [17] gave the impression that the vortex system is disturbed almost immediately after emerging from the trailing edge, resulting in the prompt core growth deduced from the phase-averaged data in Fig. 4(a). In accordance with those findings, the secondary vortices are detected within the volume containing the youngest vortices ($\varphi = 17°$).

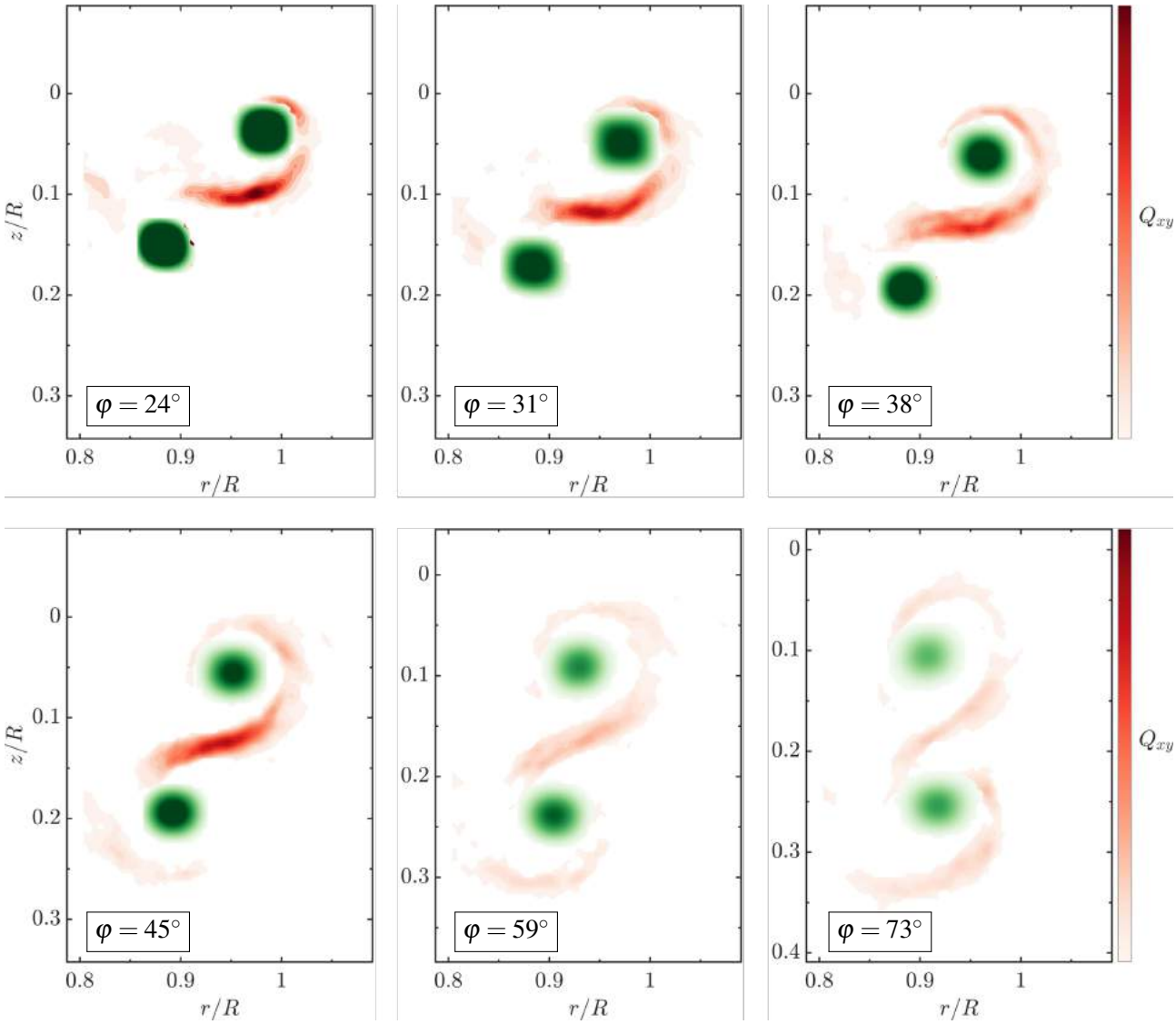


Figure 9 – Phase-averaged volumes showing the development of the primary vortices $Q_{\text{tip}}$ (green) and the secondary vortex structures $Q_{\text{sec}}$ (red) for different phase angles $\varphi$ (volumes are averaged in $t$-direction).

With regard to the findings shown in Fig. 5, it is likely that the impact of the instability and consequently the presence of secondary structures is pronounced up to a rotor phase of $\varphi \approx 60°$. Due to the lack of temporaly resolved data, a statistical approach was used to evaluate the strength of secondary vortices for each measured volume. The aforementioned decomposition of the Q-criterion was performed for all 300 snapshots recorded for each rotor phase and the results were subsequently averaged. To account for the varying position with regard to the $t$-axis of the secondary structures, an additional averaging was performed in $t$-direction over the entire volume depth. The resulting isocontours of $Q_{\text{tip}}$ and $Q_{\text{sec}}$ are shown in Fig. 9 for different rotor phases. The primary vortices identified by $Q_{\text{tip}}$ are marked in green, the averaged secondary structures are depicted with the red colour scale. A quantitative evaluation is restrained due to the unsteady characteristics of the secondary vortices within each volume. Still, a qualitative insight on the evolution of the entire vortex system is given by the deduced contours. The formation of the vortex braids start in the vicinity of the tip vortex. With proceeding phase angle, the structure of the secondary vortices expands towards the fin vortex. At a rotor phase of $\varphi = 45°$, the braid nearly entwines both primary vortices. In terms of the strength of the tip vortices, a decrease of $Q_{\text{tip}}$ is observed for increasing phase angles, in agreement with the development of the azimuthal vorticity component shown in Fig. 2(b). The statistical results confirm that the influence of the secondary structures is especially high within the early wake stages. With widening primary core radii and reduced maximum $Q_{\text{tip}}$ values, the contours start fading out ($\varphi > 45°$). Since

the actual amount of structures detected during the averaging process was not tracked, it is not clear if the strength or the total count of the secondary vortices is decreased for higher phase angles. Still, the obtained results are in good agreement with the conduct found for the phase-averaged data in 3.1. Their presence appears to be directly connected with the core growth, causing the concentrated vorticity distribution of the primary vortices to be widened.
Nevertheless, time resolved experimental data of the formation and subsequent evolution of the secondary structures is still missing. This issue will be adressed in subsequent measurement campaigns which will involve high-speed volumetric measurements. In addition, the characteristic parameters of the secondary structures are of special interest. In a follow-up study to the work of Wolf et al. [38], Schwarz et al. provided a comprehensive analysis of the secondary structures and their evolution in the wake of a two-bladed rotor in hovering conditions, combining experimental and numerical methods [40]. Higher spatial resolution allowed the extraction of the secondary vortex parameters, consequently an increased spatial resolution should also be targeted for future experiments within the presented project.

## 4 Conclusions

Within this contribution, we have presented the outcome of an experimental study containing volumetric velocity measurements of a helical vortex pair influenced by centrifugal instabilities. The vortex pair was generated by a one-bladed rotor in hover conditions, which was investigated in a water channel. A parametric fin is used to generated the secondary vortex, its geometric specifications have a direct impact on the emerging vortex system, compare [17]. The main objective of the proposed tip design is a modifaction of the rotor wake properties in order to mitigate the negative effects associated with blade-vortex interactions. Previous experimental studies showed, that the desired goal can indeed be achieved through mutual interactions and an eventual vortex merging for the generated tip vortex pair. For certain fin configurations, an imminent rapid growth of both vortex core radii before the subsequent vortex merging process was found, hinting at the presence of an instability phenomenon. It was identified as the centrifugal instability, which affects both vortices and provokes the observed growth rates. To gain new insights in the occuring flow phenomena, volumetric velocity measurements using the "Shake-The-Box" technology were performed for one chosen configuration in the early rotor wake. A comparison with previously recorded planar PIV data showed good agreement between the phase-averaged data of both measurements with regard to the extracted characteristic vortex parameters. The instability effect in terms of any occuring secondary flow structures was not detected in the volumetric phase-averaged data. Instantenous snapshots were analysed to reveal the presence of secondary vortices entangling both tip and fin vortex, comparable to the structures found in rotor wakes within the study of Wolf et al. [38]. A qualititave statistical evaluation revealed that the secondary strucures are pronounced in the early wake stages, which is in accordance with the core evolution obtained from the phase-averaged data. Their presence is directly connected to the core growth and the decreasing vorticity peaks of the primary vortices. A limited spatial resolution impeded the determination of valid vortex parameters for the secondary vortices, an improvement will be targeted in future measurements. In addition, time-resolved volumetric STB is planned to gain new insights in the formation and development of the structures. With regard to the occurence of the centrifugal instability, its physical origin still remains unclear. To address this issue, a new rotor geometry providing a different radial circulation distribution will be investigated in the future.

## Acknowledgements

This work is part of the German-French project TWIN-HELIX, supported by the *Deutsche Forschungsgemeinschaft* (grant no. 391677260) and the French *Agence Nationale de la Recherche* (grant no. ANR-17-CE06-0018).

## Contact Author Email Address

The contact author email address is: dominic.schroeder@ilr.rwth-aachen.de

## Copyright Statement



## References

[1] Y. Yu. “Rotor blade–vortex interaction noise”. In: *Progress in Aerospace Sciences* 36.2 (2000), pp. 97–115.

[2] A. R. George. “Helicopter Noise: State-of-the-Art”. In: *Journal of Aircraft* 15.11 (1978), pp. 707–715.

[3] F. H. Schmitz and Y. H. Yung. “Helicopter impulsive noise: Theoretical and experimental status”. In: *Journal of Sound and Vibration* 109.3 (1986), pp. 361–422.

[4] J. C. Hardin and S. L. Lamkin. “Concepts for reduction of blade/vortex interaction noise”. In: *Journal of Aircraft* 24.2 (1987), pp. 120–125.

[5] J. N. Sørensen. “Instability of helical tip vortices in rotor wakes”. In: *Journal of Fluid Mechanics* 682 (2011), pp. 1–4.

[6] L. J. Vermeer, J. N. Sørensen, and A. Crespo. “Wind turbine wake aerodynamics”. In: *Progress in Aerospace Sciences* 39.6-7 (2003), pp. 467–510.

[7] H. U. Quaranta et al. “Local and global pairing instabilities of two interlaced helical vortices”. In: *Journal of Fluid Mechanics* 863 (2019), pp. 927–955.

[8] M. Felli, R. Camussi, and F. Di Felice. “Mechanisms of evolution of the propeller wake in the transition and far fields”. In: *Journal of Fluid Mechanics* 682 (2011), pp. 5–53.

[9] J. N. Sørensen, I. V. Naumov, and V. L. Okulov. “Multiple helical modes of vortex breakdown”. In: *Journal of Fluid Mechanics* 683 (2011), pp. 430–441.

[10] A. Bauknecht et al. “Blade tip vortex measurements on actively twisted rotor blades”. In: *Experiments in Fluids* 58.5 (2017), p. 301.

[11] P. Meunier, S. Le Dizès, and T. Leweke. “Physics of vortex merging”. In: *Comptes Rendus Physique* 6.4-5 (2005), pp. 431–450.

[12] M. V. Melander, N. J. Zabusky, and J. C. Mcwilliams. “Symmetric vortex merger in two dimensions: causes and conditions”. In: *Journal of Fluid Mechanics* 195 (1988), pp. 303–340.

[13] C. Cerretelli and C. H. K. Williamson. “The physical mechanism for vortex merging”. In: *Journal of Fluid Mechanics* 475 (2003), pp. 41–77.

[14] P. Meunier and T. Leweke. “Three-dimensional instability during vortex merging”. In: *Physics of Fluids* 13.10 (2001), pp. 2747–2750.

[15] A. Brocklehurst and G. N. Barakos. “A review of helicopter rotor blade tip shapes”. In: *Progress in Aerospace Sciences* 56 (2013), pp. 35–74.

[16] Y. Ostovan, M. T. Akpolat, and O. Uzol. “Experimental Investigation of the Effects of Winglets on the Tip Vortex Behavior of a Model Horizontal Axis Wind Turbine Using Particle Image Velocimetry”. In: *Journal of Solar Energy Engineering* 141.1 (2019).

[17] D. Schröder et al. “Experiments on helical vortex pairs in the wake of a rotor”. In: *AIAA Scitech 2021 Forum*. AIAA Scitech 2021 Forum. 2021.

[18] D. Schröder et al. “Instability and merging of a helical vortex pair in the wake of a rotor”. In: *Journal of Physics: Conference Series* 1934.1 (2021), p. 012007.

[19] T. Leweke, S. Le Dizès, and C. H. Williamson. “Dynamics and Instabilities of Vortex Pairs”. In: *Annual Review of Fluid Mechanics* 48.1 (2016), pp. 507–541.

[20] V. L. Okulov. “On the stability of multiple helical vortices”. In: *Journal of Fluid Mechanics* 521 (2004), pp. 319–342.

[21] H. U. Quaranta, H. Bolnot, and T. Leweke. “Long-wave instability of a helical vortex”. In: *Journal of Fluid Mechanics* 780 (2015), pp. 687–716.

[22] F. J. Blanco-Rodríguez and S. Le Dizès. “Elliptic instability of a curved Batchelor vortex”. In: *Journal of Fluid Mechanics* 804 (2016), pp. 224–247.

[23] F. J. Blanco-Rodríguez and S. Le Dizès. “Curvature instability of a curved Batchelor vortex”. In: *Journal of Fluid Mechanics* 814 (2017), pp. 397–415.

[24] Y. Hattori and Y. Fukumoto. “Short-wave stability of a helical vortex tube: the effect of torsion on the curvature instability”. In: *Theoretical and Computational Fluid Dynamics* 24.1 (2010), pp. 363–368.

[25] T. Leweke et al. “Long- and short-wave instabilities in helical vortices”. In: *Journal of Physics: Conference Series* 524.1 (2014), p. 012154.

[26] B. J. Bayly. “Three–dimensional centrifugal–type instabilities in inviscid two–dimensional flows”. In: *The Physics of Fluids* 31.1 (1988).

[27] P. Billant and F. Gallaire. “A unified criterion for the centrifugal instabilities of vortices and swirling jets”. In: *Journal of Fluid Mechanics* 734 (2013), pp. 5–35.

[28] P. Billant and F. Gallaire. “Generalized Rayleigh criterion for non-axisymmetric centrifugal instabilities”. In: *Journal of Fluid Mechanics* 542 (2005), pp. 365–379.

[29] D. Schröder et al. “Experimental investigation of a rotor blade tip vortex pair”. In: *CEAS Aeronautical Journal* 36 (2021), p. 97.

[30] D. Schanz, S. Gesemann, and A. Schröder. “Shake-The-Box: Lagrangian particle tracking at high particle image densities”. In: *Experiments in Fluids* 57.5 (2016), p. 1393.

[31] A. K. Prasad and K. Jensen. “Scheimpflug stereocamera for particle image velocimetry in liquid flows”. In: *Applied optics* 34.30 (1995), pp. 7092–7099.

[32] B. Wieneke. “Volume self-calibration for 3D particle image velocimetry”. In: *Experiments in Fluids* 45.4 (2008), pp. 549–556.

[33] D. Schanz et al. “Non-uniform optical transfer functions in particle imaging: calibration and application to tomographic reconstruction”. In: *Measurement Science and Technology* 24.2 (2013), p. 024009.

[34] W. J. Devenport et al. “The structure and development of a wing-tip vortex”. In: *Journal of Fluid Mechanics* 312 (1996), pp. 67–106.

[35] van der Wall, Berend G. and H. Richard. “Analysis methodology for 3C-PIV data of rotary wing vortices”. In: *Experiments in Fluids* 40.5 (2006), pp. 798–812.

[36] J. Jeong and F. Hussain. “On the identification of a vortex”. In: *Journal of Fluid Mechanics* 285.1 (1995), pp. 69–94.

[37] J. C. R. Hunt, A. Wray, and P. Moin. “Eddies, streams, and convergence zones in turbulent flows”. In: *Proceedings of the Summer Program*. 1988.

[38] C. C. Wolf et al. “Experimental study of secondary vortex structures in a rotor wake”. In: *Experiments in Fluids* 60.11 (2019), p. 49.

[39] B. Gibeau, C. R. Koch, and S. Ghaemi. “Secondary instabilities in the wake of an elongated two-dimensional body with a blunt trailing edge”. In: *Journal of Fluid Mechanics* 846 (2018), pp. 578–604.

[40] C. Schwarz et al. “Development of secondary vortex structures in rotor wakes”. In: *Experiments in Fluids* 63.1 (2022).